JACS
JOURNAL OF THE AMERICAN CHEMICAL SOCIETY

Article

Generation of N-Centered Radicals via a Photocatalytic Energy Transfer: Remote Double Functionalization of Arenes Facilitated by Singlet Oxygen

Vineet Kumar Soni, Ho Seong Hwang, Yu Kyung Moon, Sung-Woo Park, Youngmin You, and Eun Jin Cho

J. Am. Chem. Soc., **Just Accepted Manuscript** • DOI: 10.1021/jacs.9b05572 • Publication Date (Web): 07 Jun 2019

Just Accepted

is published by the American Chemical Society. 1155 Sixteenth Street N.W., Washington, DC 20036

Generation of N-Centered Radicals via a Photocatalytic Energy Transfer: Remote Double Functionalization of Arenes Facilitated by Singlet Oxygen

Vineet Kumar Soni,[a] Ho Seong Hwang,[a] Yu Kyung Moon,[b] Sung-Woo Park,[c] Youngmin You,[b*] and Eun Jin Cho[a*]

[a]Department of Chemistry, Chung-Ang University, 84 Heukseok-ro, Dongjak-gu, Seoul 06974, Republic of Korea

[b]Division of Chemical Engineering and Materials Science, Ewha Womans University, Seoul 03760, Korea.

[c]Center for Catalytic Hydrocarbon Functionalizations, Institute for Basic Science (IBS), and Department of Chemistry, Korea Advanced Institute of Science and Technology (KAIST), Daejeon 34141, Republic of Korea.

KEYWORDS: photocatalysis, energy transfer, N-radical cascade, remote functionalization, singlet oxygen

ABSTRACT: An unprecedented approach for the generation of N-centered radical via a photocatalytic energy transfer process from readily available heterocyclic precursors is reported, which is distinctive to the previous electron transfer approaches. In combination with singlet oxygen, the *in situ* generated nitrogen radical from oxadiazoline substrate in the presence of *fac*-Ir(ppy)$_3$ undergoes a selective *ipso*-addition to arenes to furnish remotely double functionalized spiro-azalactam products. The mechanistic studies provide compelling evidence that the catalytic cycle selects the energy transfer pathway. A concurrent activation of molecular oxygen to generate singlet oxygen by energy transfer is also rationalized. Furthermore, the occurrence of electron transfer phenomenon is excluded based on the negative driving forces for one-electron transfer between oxadiazoline and the excited state of *fac*-Ir(ppy)$_3$ with consideration to their redox potentials. The necessity of singlet oxygen as well as the photoactivated oxadiazoline substrate is clearly supported by a series of controlled experiments. Density functional studies have also been carried out to support these observations. The scope of substrates is explored by synthesizing diversely functionalized cyclohexadienone moieties in view to their utility in complex organic syntheses and as potential targets in pharmacology.

1. INTRODUCTION

Heterocycles are prevalent structural motifs finding versatile utilities in various research areas due to their interesting biological activities and unique physical properties.[1] As a result, the development of more efficient and preparative synthetic routes to common heterocycles has been a special interest in synthetic chemistry.[2] While linear synthetic approaches are predominantly utilized to prepare heterocycles at present,[3] a transformative strategy to access heterocycles of interest from another type of more readily available heterocycles is less explored mainly due to lack of effective synthetic methodologies.[4,5] Considering the fact that the structural variation of privileged heterocycles continues to draw extensive synthetic efforts,[6] the envisioned transformations between structurally distinct heterocycles would be highly interesting if additional functional groups can be introduced during the course of such interconversions.

In recent years, visible-light induced photocatalysis has emerged as a powerful synthetic tool,[7,8] thus often replacing the conventional lengthy preparative approaches. In particular, the generation of *N*-centered radicals under mild photocatalytic conditions has enabled an access to azaheterocycles in an unprecedentedly concise manner.[9] Recently, the use of amines as N-radical precursor has evolved as highly atom-economic strategy.[10,11] However, many of currently available photocatalytic procedures still employ pre-activated amino precursors as the indirect source of N-radical species, where a single electron transfer process reductively cleaves weak N–N, N–O, or N–X bonds (Scheme 1a).[12,13] The critical drawback of these methods is the generation of stoichiometric amounts of by-products released from the pre-functionalized amino precursors. Herein, we envisioned a new strategy of generating N-centered radical directly from a readily available oxadiazoline heterocycle, leading to the generation of new azaheterocycles in an atom-econmical manner (Scheme 1b). The choice of oxadiazolines as N-radical precursors is based on the following desirable features: (i) the N-O bonds in certain heterocycles such as oxadiazoles can be activated by photoirradiation[14,15]; (ii) the leaving groups can also incorporate into the product skeleton without generation of wastes; and (iii) as radical precursors, oxadiazolines can be easily accessed with variation of substituents, eventually allowing for a

product diversification.

At the outset of our studies, we predicted that 5-aryl-1,2,4-oxadiazoline **1** may undergo the desired ring cleavage by the photoactivation to form an iminyl radical that will subsequently cyclize at the *ortho*-position of the pendent phenyl moiety to give rise to quinazolinone products via the homolytic aromatic substitution (HAS).[15c,16] However, the reaction turned out to follow an *unprecedented pathway* furnishing spiro-azalactam compounds with remote oxygenation under oxygen atmosphere (Scheme 1c).[17] This result is especially notable in that C–N bond-forming dearomatization of arenes is less explored.[18]

Scheme 1. Generation of N-Centered Radicals

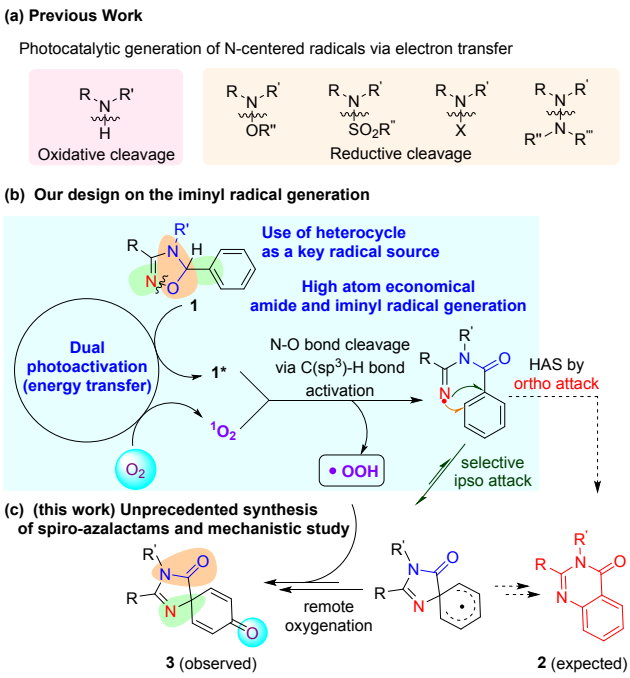

Arene dearomatization has been highlighted as a powerful transformation that generates complex molecules, including spirocyclohexadienones.[19] Notably, the presence of spirocyclohexadienone moiety in natural products[19c] and such diazaspiro compounds as potential pharmaceutical agents have already been highlighted.[20]

Herein, we describe the first example of utilizing heterocycles as an iminyl radical precursor under visible-light photocatalytic conditions. More importantly, unlike the previous procedures of generating N-cantered radicals via an electron transfer process, the present iminyl radical formation has been elucidated to proceed through energy-transfer pathways. This process not only generates cyclohexadienone moiety from simple arene ring [21] but also amide and amino moieties to provide highly functionalized spiro-azalactams. The mechanism was investigated in detail by performing photophysical and electrochemical measurements, as well as computational studies.

2. RESULTS AND DISCUSSION

2.1. Reaction Development.

To verify our working hypothesis, a readily available 5-aryl-1,2,4-oxadiazoline derivative **1a** was subjected to the photocatalysis conditions, by using either complexes containing transition metals (Ru, Ir, or Pt) or organic dyes (Eosin Y). Visible light was irradiated from a 23 W compact fluorescent lamp (CFL) at a concentration of 0.2 M in DMSO at 20~22 °C under oxygen atmosphere (Table 1). To our surprise, the initially expected quinazolinone[15c] **2a** was formed in minor (10%) while a major product was spiro-azalactam **3a** (40%) when $[Ru(bpy)_2]Cl_2$ was employed as a photocatalyst (entry 1). This unexpected product was formed in slightly higher yield especially when *fac*-$Ir(ppy)_3$ and $[Ir\{dF(CF_3)ppy\}_2(dtbpy)]PF_6$ were used among different photocatalysts examined (entries 2–9), and more easily accessible *fac*-$Ir(ppy)_3$ was chosen for further optimization. The reaction was found to be rather sensitive to solvents, and DMSO was more effective than any others examined (entries 10–13). Control experiments revealed that the reaction was completely ineffective in the absence of light or photocatalyst (entries 14-16).

Table 1. Optimization Studies[a]

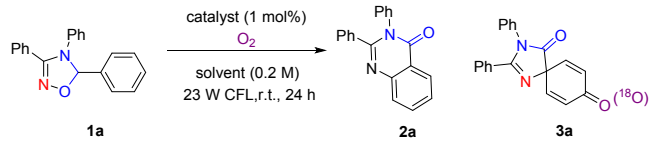

entry	catalyst	solvent	variations	yield (%)[b] 2a	yield (%)[b] 3a[c]
1	$[Ru(bpy)_3]Cl_2$	DMSO	-	11	40 (25)
2	$[Ru(phen)_3]Cl_2$	DMSO	-	13	39 (40)
3	*fac*-Ir(ppy)$_3$	DMSO	-	10	55
4	$[Ir(dtbbpy)(ppy)_2]PF_6$	DMSO	-	6	22 (15)
5	$[Ir\{dF(CF_3)ppy\}_2(dtbpy)]PF_6$	DMSO	-	12	56
6	*fac*-Ir(dFppy)$_3$	DMSO	-	15	28 (24)
7	Pt(ppy)acac	DMSO	-	5	15 (58)
8	Eosin Y	DMSO	-	12	25 (16)
9	TPPT	DMSO	-	3	20 (68)
10	*fac*-Ir(ppy)$_3$	MeCN	-	-	7 (82)
11	*fac*-Ir(ppy)$_3$	$CHCl_3$	-	-	0 (94)
12	*fac*-Ir(ppy)$_3$	DMF	-	13	46
13	*fac*-Ir(ppy)$_3$	DMA	-	8	26 (20)
14	*fac*-Ir(ppy)$_3$	DMSO	no hv	-	- (96)
15	-	DMSO	no catalyst	-	- (92)
16	-	DMSO	no catalyst, 365 nm	-	- (91)
17	*fac*-Ir(ppy)$_3$	DMSO	no O_2	-	- (22)
18	*fac*-Ir(ppy)$_3$	DMSO	DIPEA (0.2 eq)	20	54
19	***fac*-Ir(ppy)$_3$**	**DMSO**	**K_2CO_3 (0.2 eq)**	5	**70** [69][d]
20	*fac*-Ir(ppy)$_3$	DMSO	Cs_2CO_3 (0.2 eq)	14	39 (8)
21	*fac*-Ir(ppy)$_3$	DMSO	K_2CO_3 (0.1 eq)	8	64 (5)
22	*fac*-Ir(ppy)$_3$	DMSO	K_2CO_3 (0.5 eq)	9	48 (16)
23	*fac*-Ir(ppy)$_3$	DMSO	K_2CO_3 (0.2 eq), 0.1 M	10	58 (3)
24	***fac*-Ir(ppy)$_3$**	**DMSO**	**K_2CO_3 (0.2 eq), 0.5 M**	6	**70**
25	*fac*-Ir(ppy)$_3$	DMSO	K_2CO_3 (0.2 eq), Blue LEDs	16	50
26	*fac*-Ir(ppy)$_3$	DMSO	K_2CO_3 (0.2 eq), White LEDs	24	65
27	*fac*-Ir(ppy)$_3$	DMSO	K_2CO_3 (0.2 eq), 10 °C	3	33 (60)
28	*fac*-Ir(ppy)$_3$	DMSO	K_2CO_3 (0.2 eq), 50 °C	18	50
29	*fac*-Ir(ppy)$_3$	DMSO	K_2CO_3 (0.2 eq), 0.5 mol% cat.	6	54

[a]Reaction scale: 0.1 mmol. [b]^{1}H NMR yields using bromoform as the internal standard. [c]Yields of recovered **1a** in parentheses. [d]Yield of **3a** in parenthesis under $^{18}O_2$ atmosphere. TPPT = 2,4,6-triphenylpyrylium tetrafluoroborate.

The use of molecular oxygen was crucial for the formation of **3a** to confirm that it is the oxygen source incorporated

at the *para*-position (entry 17). The effect of additives on product yields was also examined (entries 18-22); wherein, a sub-equivalent amount of K_2CO_3 (20 mol %) increased the product yield of **3a** (70%) with higher *ipso*-selectivity (entry 19). Though the diluted reaction mixture provided less product yield, a relatively higher concentration did not affect the reaction efficiency (entries 23 and 24). In addition, CFL was found to be the best photon source in this transformation, and the reaction was optimal at room temperature (entries 25 and 26). Any alteration in reaction temperature was not helpful (entries 27 and 28). The lower catalyst loading (0.5 mol %) decreased the yield of **3a** (entry 29). An isotopic labelling experiment with $^{18}O_2$, where the product with ^{18}O was exclusively formed from the reaction, clearly confirmed that molecular oxygen is the actual source of oxygen in this process.

Interestingly, highly relevant 3,5-diphenyl-1,2,4-oxadiazole (aromatic variant) was not a suitable iminyl radical source under the above optimized conditions, indicating a different mode of activation with **1a**. (Scheme S1). Previously, Pace, Vivona, and coworkers explored photochemical reactions of oxadiazoles where nitrene or iminyl radicals were generated by N-O bond cleavage under UV irradiation.[14]

Scheme 2. Mechanistic Investigations

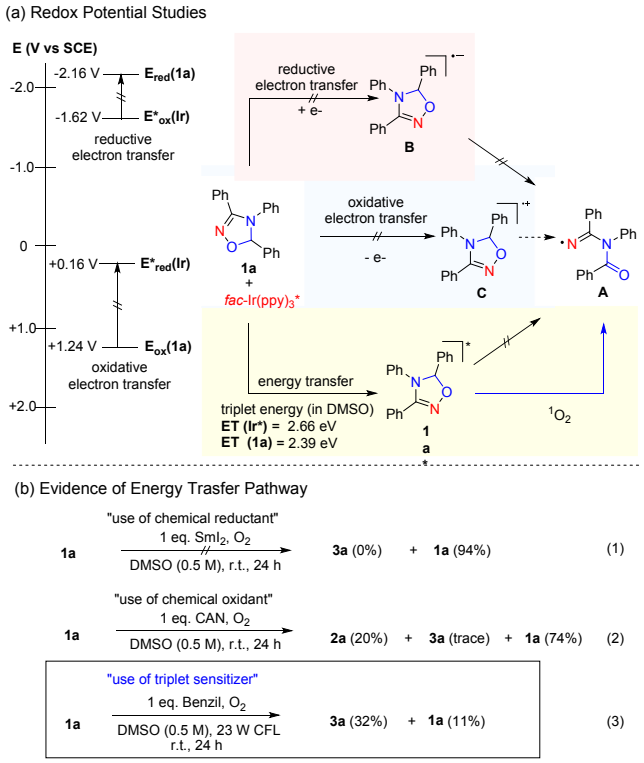

2.2. Mechanistic Studies and Proposal.

To ascertain mechanistic insights, we performed electrochemical investigations. The irreversible oxidation of **1a** was observed at 1.24 V vs SCE (Figure S1). This value was more positive than the excited-state reduction potential (E^*_{red}, 0.16 V vs SCE) of 2.0 mM *fac*-Ir(ppy)$_3$ (DMSO), revealing an endoergic electron transfer from **1a** to the excited-state *fac*-Ir(ppy)$_3$ (*fac*-Ir(ppy)$_3$*). A comparison between the reduction potential of 2.0 mM **1a** (–2.16 V vs SCE, DMSO) and the excited-state oxidation potential (E^*_{ox}, –1.62 V vs SCE) of *fac*-Ir(ppy)$_3$* also indicated thermodynamic forbiddance of reductive electron transfer from *fac*-Ir(ppy)$_3$* to **1a**. These results permitted us to exclude electron-transfer pathways to the generation of radical intermediates **B** or **C** (Scheme 2a).[22,23] Furthermore, attempts to replicate the aza-lactam synthesis with standard chemical one-electron reductant (SmI_2) or oxidant (ceric ammonium nitrate) did not afford **3a**, ruling out the electron transfer pathways [Scheme 2b(1) and (2)].

Our TD–DFT calculations predicted an occurrence of triplet–triplet energy transfer (TTET) from the *fac*-Ir(ppy)$_3$* to **1a** because the triplet state energy (E_T) of the former (2.66 eV) was greater than that (2.39 eV) of the latter (Scheme 2a).[24] The use of benzil (E_T = 2.57 eV)[24] as a triplet sensitizer instead of *fac*-Ir(ppy)$_3$ provided **3a**, corroborating this energy-transfer hypothesis [Scheme 2b(3)].[25] The energy-transfer interaction was verified by monitoring phosphorescence decay traces of *fac*-Ir(ppy)$_3$ (100 μM in Ar-saturated DMSO) using time-correlated single-photon-counting techniques with increasing concentration of **1a** ([**1a**]). As shown in Figure 1a, the phosphorescence lifetime decreased in proportion with [**1a**]. A linear fit of the phosphorescence quenching rate ($1/\tau_{obs}$(**1a**) – $1/\tau_{obs}$, where τ_{obs}(**1a**) and τ_{obs} correspond to the phosphorescence lifetimes in the absence and presence of **1a**) *vs.* [**1a**] returned the rate constant for bimolecular quenching (k_Q) to be 1.8 × 10^7 M^{-1}s^{-1}. Since electron transfer was disfavoured, the k_Q value can be equated as the rate constant for energy transfer to **1a** (k_{ET}(**1a**)).

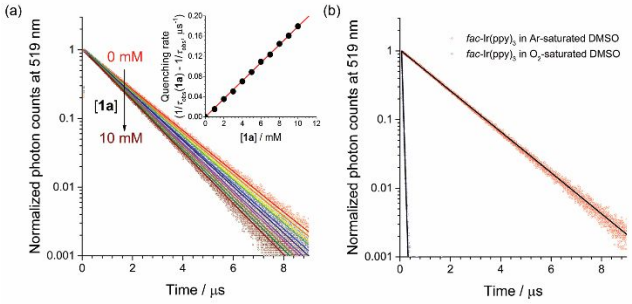

Figure 1. Phosphorescence decay traces of 100 μM *fac*-Ir(ppy)$_3$ in DMSO. (a) Decay traces acquired for Ar-saturated solutions with increasing concentration of **1a**. The inset graph depicts the pseudo linear plot of the quenching rate ($1/\tau_{obs}$(**1a**) – $1/\tau_{obs}$) *vs* the concentration of **1a**. (b) Decay traces acquired in the absence of **1a** before (red) and after (blue) O_2 saturation.

Although **1a** and *fac*-Ir(ppy)$_3$ had a certain spectral overlap (Figure S2), Förster-type energy transfer was predicted to be insignificant at our reaction conditions (i.e., 0.2-0.5 M **1a** and 2 mM *fac*-Ir(ppy)$_3$). The rate for bimolecular energy transfer (ET rate) is proportional to [**1a**]^2 in the Förster-type energy transfer regime (i.e., Förster ET rate ∝ [**1a**]^2), given that the solution is homogeneous.[26] On the contrary, the Dexter-type energy transfer regime possesses a linear relationship between

ln(ET rate) and $[\mathbf{1a}]^{-1/3}$. We took the phosphorescence quenching rate (Figure 1a) as the ET rate because quenching by photoinduced electron transfer was forbidden (*vide supra*). As shown in Figure 2a, the ET rate displays a linearity in the Dexter-type energy transfer region of $[\mathbf{1a}]^{-1/3} < 6.2$ $M^{-1/3}$. This value corresponds to [**1a**] > 4.1 mM. The linearity of the ET rate in the Förster-type energy transfer is observed at $[\mathbf{1a}]^2 < 10^1$ mM^2 (i.e., [**1a**] < 3.2 mM) (Figure 2b). Comparing the limiting concentrations with the reaction concentration ([**1a**] = 0.2-0.5 M), we conclude that Dexter-type energy transfer was dominant. This conclusion was consistent with the TD–DFT calculation results which predicted triplet states were involved in the energy transfer.

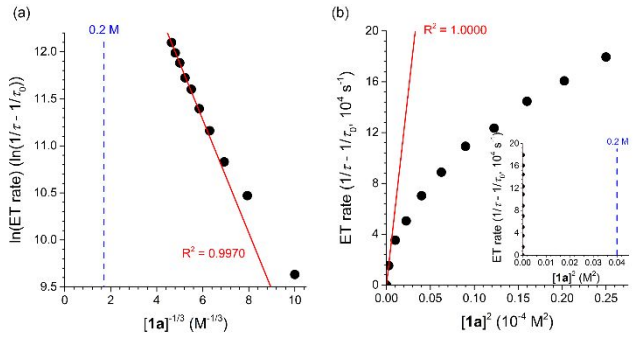

Figure 2. Energy transfer mechanism. (a) A plot of the natural logarithm of the energy transfer (ET) rate as a function of $[\mathbf{1a}]^{-1/3}$. The red line shows a visual guidance where the Dexter ET mechanism applies (i.e., Dexter regime; ln(ET rate) $\propto$ $[\mathbf{1a}]^{-1/3}$). The vertical blue line corresponds to [**1a**] employed for the reaction. (b) A plot of the energy transfer (ET) rate as a function of $[\mathbf{1a}]^2$. The red line shows a visual guidance where the Förster ET mechanism applies (i.e., Förster regime; ET rate $\propto$ $[\mathbf{1a}]^2$). The inset graph compares [**1a**] employed for the reaction (vertical blue line) and the Förster ET regime.

The implausibility of generating highly unstable diradical species by direct homolytic N-O bond cleavage of **1a*** led us to examine the distinctive pathway involving singlet oxygen ($^1O_2$) to yield **A**.[27] The participation of singlet oxygen in the current process was rationalized by several experiments. The use of singlet oxygen scavenger, such as DABCO or NaN_3, retarded the reaction. The results provide strong evidence for the key role of singlet oxygen in the transformation [Scheme 3(1)]. Furthermore, the non-reactivity of a sterically demanding substrate, i.e. 2,6-disubstituted phenyl derivative (**1b**) suggested the primary involvement of singlet oxygen in the iminyl radical generation [Scheme 3(2)]. We observed a significant decrease in τ_{obs} (1.46 μs → 0.037 μs) upon O_2 equilibration (Figure 1b). The corresponding rate for energy transfer from *fac*-Ir(ppy)$_3$ to O_2 (ET rate(O_2)) was estimated to 2.6×10^6 s^{-1}. Note that this value was comparable to the energy-transfer rate to **1a** (ET rate(**1a**)) at a concentration of 0.5 M (i.e., ET rate(**1a**) = k_{ET}(**1a**) × 0.5 M = 9.0×10^6 s^{-1}). Both energy-transfer pathways were one order of magnitude faster than the intrinsic decay rate of the excited state of *fac*-Ir(ppy)$_3$ (5.9×10^5 s^{-1}), supporting the dual activation of **1a** and O_2. The photosensitization of $^1O_2$ by *fac*-Ir(ppy)$_3$ was evidenced by using 1,3-diphenylisobenzofuran (DPBF), a $^1O_2$ probe, where the quantum yield for $^1O_2$ sensitization (Φ_Δ) was as high as 0.95 (Figure 3; see SI for details).

Scheme 3. Role of Singlet Oxygen

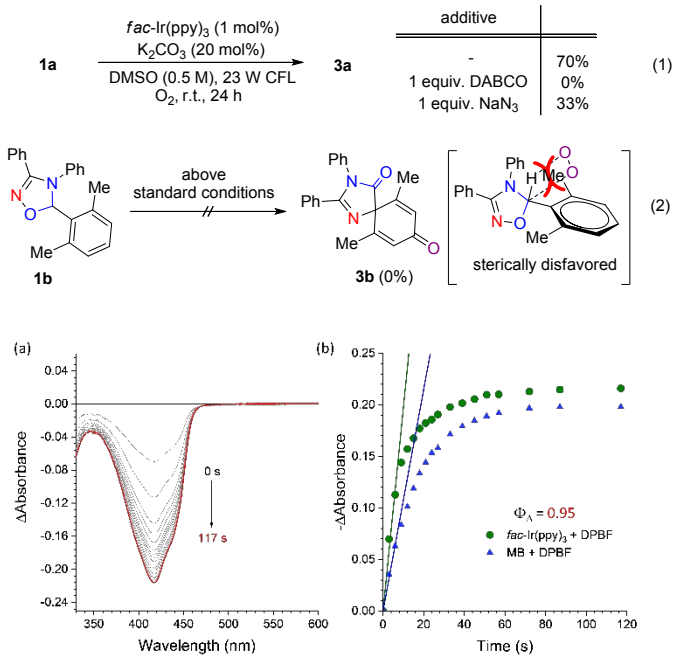

Figure 3. (a) UV–vis absorption difference spectra of an O_2-saturated DMSO solution containing 10 μM DPBF and 100 μM *fac*-Ir(ppy)$_3$ recorded during continuous photoirradiation of white light using a Xenon lamp. (b) Plots depicting the absorbance difference of DPBF at 412 nm as a function of photoirradiation time. Methylene blue (MB) as an external reference. The straight lines are the linear fits to the initial three points.

Our mechanism involving double photon excitation of **1a** and O_2 is unique. To assess our mechanism, we ran the reaction of **1a** with varying the photon flux ($0.21–3.6 \times 10^{-8}$ einstein s^{-1}). It was found that the concentration of **3a** ([**3a**]) increased non-linearly with the photon flux (Figure S4). This observation served as a strong indication of the involvement of two photons for the double excitation of **1a** and O_2. On the contrary, the quantum yield for the reaction, which was determined using the standard ferrioxalate actinometry, remained the same during the photoirradiation (16% at 6 h of photoirradiation and 18% at 30 h of photoirradiation). The quantum yield not exceeding 50% may exclude the possibility of any propagation process, e.g. involving hydrogen abstraction from **1a** by *in situ* generated hydroperoxide radical. We further confirmed this by the on–off switching of the light source during the reaction, where no further progress was observed in the dark.[28]

In addition, reactions in the presence of singlet oxygen were conducted under non-photocatalytic conditions.

The reaction of **1a** with *in situ* generated singlet oxygen in dark under photocatalyst-free conditions did not yield any product even after 24 h, suggesting a crucial involvement of **1a*** in the transformation (Scheme 4a).[29] The reaction of **1a** and benzoyl peroxide at 80 °C under oxygen atmosphere proceeded with low reactivity and selectivity, as only 10% of **3a** was formed along with **2a** (31%) and unreacted **1a** (51%) (Scheme 4b), showing the advantage of visible light-mediated photocatalytic processes in efficient synthesis of spiro-azalactams.

Scheme 4. Control Experiments with singlet oxygen or peroxide

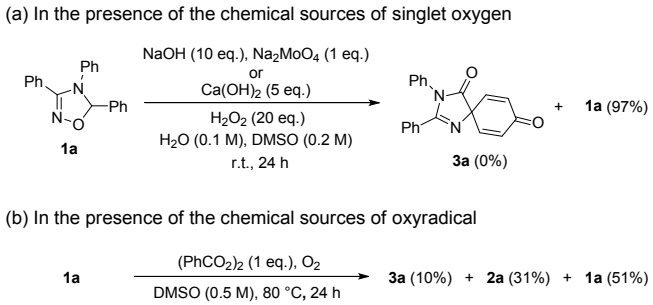

Based on the above observations, a plausible mechanistic pathway for the current transformation is depicted in Scheme 3a. First, *fac*-Ir(ppy)$_3$ photosensitize **1a** and molecular oxygen into **1a*** and $^1O_2$, respectively, via energy transfer. A dehydrogenative insertion of singlet oxygen at the 5-position of **1a*** follow to generate a hydroperoxy species **D***. The homolytic N–O bond cleavage in **D*** is assumed to take place smoothly to generate a key iminyl radical **A**, along with hydroperoxide radical (HOO$^\bullet$). We propose that an *ipso* attack of the N-centered radical of **A** is kinetically feasible to furnish a spirocyclic species **E** that will recombine with HOO$^\bullet$ or O_2 at the *para*-position selectively, eventually producing **3a** via a cyclohexadienyl hydroperoxide species **F** with a release of water. Although the spin density values for spirocyclic radical **E** suggests more favored *para* attack by HOO$^\bullet$ or O_2 [para (0.605) vs ortho (0.415)], the *ortho*-hydroperoxidation followed by [1,3]-sigmatropic shift is also plausible under the photochemical conditions.[30] This mechanistic postulate was further supported by DFT calculations (Scheme 3b, Figure S5). The electronic environment of **D*** induces the favorable spin density on the bonded nitrogen and oxygen atoms to facilitate the homolytic N-O bond cleavage with concurrent exclusion of hydroeproxide radical leading to a low energy iminyl radical species **A**. Although all attempts to detect hydroperoxide intermediate **F** were not fruitful, the presence of peroxide was observed during the course of reaction.[31]

2.3. Substrate Scope.

Next, the generality of the transformation was investigated by applying various types of substrates under the optimized conditions (Table 2).

Scheme 5. Proposed Mechanism and DFT Studies

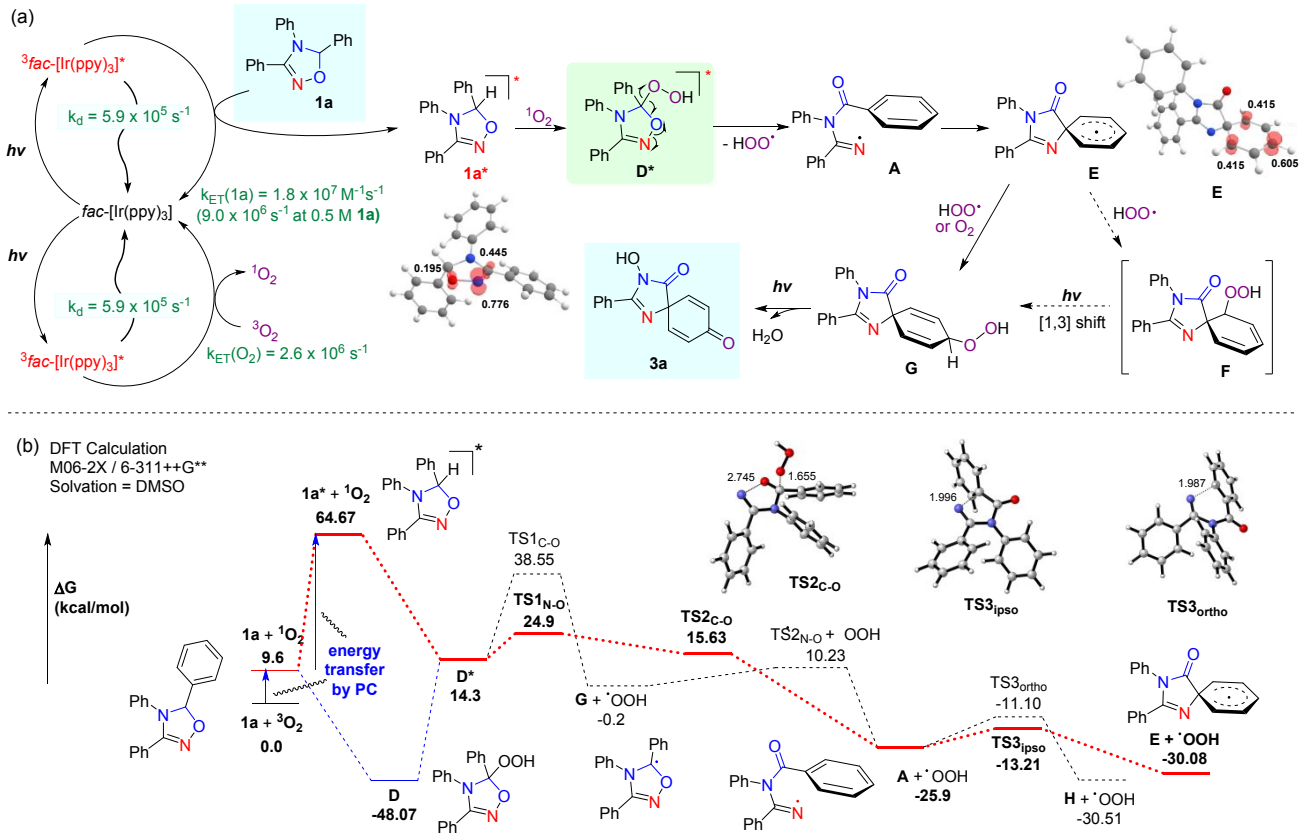

Table 2. Substrate Scope[a]

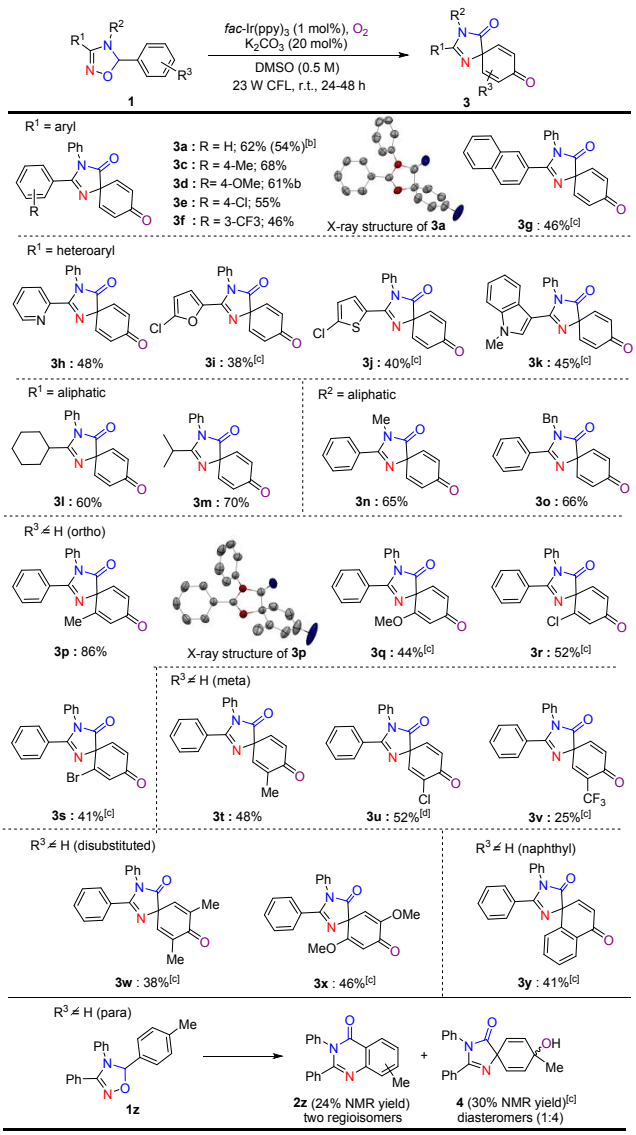

[a]Reactions were performed on a 0.3 mmol scale, and the isolated yields are reported; [b]7 mmol scale after 96 h; [c]96 h reaction time; [d]72 h reaction time.

The scope of substituents R^1 at the 3-position in 1,2,4-oxadiazolines **1** was first examined. Substrates with aromatic substituents, including a naphthyl group, underwent the desired oxygenative dearomatization in satisfactory efficiency, to give the corresponding spiro-azalactams (**3a, 3c–3g**). Heteroaryl substituents, such as pyridyl, furyl, thiophenyl, and indolyl, were also found to be compatible with the present condi tions (**3h–3k**). The applicability of the present method was further demonstrated by installing aliphatic groups (**3l, 3m**). Variation at the 4-position (R^2) in 1,2,4-oxadiazolines was also plausible, where *N*-methyl and *N*-benzyl substituents were readily integrated into the products (**3n** and **3o**). In view to synthesize diversely functionalized cyclohexadienone moieties,[19] substrates containing electron-donating or withdrawing substituents on the aryl ring at the 5-position of the 1,2,4-oxadiazoline were reacted. Cyclohexadienone rings functionalized at the *ortho* and *meta* positions including naphthyl derivatives (**3p–3y**) were successfully synthesized. The structure of products **3a** and **3p** was unambiguously confirmed by X-ray crystallography (Figure S6 and S7).[32] In most cases, quinazolinone derivatives (**2**) were detected as the side products. In the case of a *para*-substituted derivative **1z**, the hydroxyl compound **4** was formed in 30% NMR yield along with two regioisomers of quinazolinones **2z**. The scale-up of **3a** from **1a** at 7 mmol scale was found to be straightforward, despite the slower conversion (54% conversion after 96 h reaction).

3. CONCLUSION

In conclusion, we herein have reported an unprecedented approach to N-centered radical from heterocycles to induce a cascade double functionalization of arenes to furnish spiro-azalactams. The reaction proceeds under mild photocatalytic conditions via an energy transfer process where photoexcited hydroperoxide initiates the homolytic N-O bond cleavage of heterocycles to induce an *ipso* attack of the resultant iminyl radical with the concomitant *para*-oxygenation of molecular oxygen. The use of simple arenes indicates high potential use of the method in late-stage modifications to achieve high levels of molecular complexity. The easy accessibility of substrates, mild reaction conditions, high functional-group tolerance, and facile formation of diversified spiro-azalactam products will give an opportunity to find its applications in synthetic and medicinal chemistry. Furthermore, the photocatalytic activation of such heterocycle offers tremendous potential for applications in other useful transformations.

ASSOCIATED CONTENT

The Supporting Information is available free of charge via the Internet at http://pubs.acs.org."
Experimental procedures, characterization of products, and spectroscopic data (PDF)
Crystallographic data for **3a** and **3p** (CIF)

AUTHOR INFORMATION

Corresponding Author

*E-mail: ejcho@cau.ac.kr (E. J. Cho)
ORCID: 0000-0002-6607-1851

*E-mail: odds2@ewha.ac.kr (Y. You)
ORCID: 0000-0001-5633-6599

Notes

The authors declare no competing financial interest.

ACKNOWLEDGMENT

We gratefully acknowledge the National Research Foundation of Korea [NRF-2012M3A7B4049657, NRF-2014011165, NRF-2017R1A2B2004082, and NRF-2019R1A2C2003969]. We thank Hongil Jo (Chung-Ang University) for help with X-ray crystallography and Prof. Sukbok Chang (KAIST) for the critical advice and guidance for the manuscript.

REFERENCES

1. For relevant books and reviews, see: (a) Quin, L. D.; Tyrell, J. A. Fundamentals of heterocyclic chemistry: importance in nature and in the synthesis of pharmaceuticals. John Wiley & Sons, 2010. (b) Joule, J. A.; Mills, K. Heterocyclic chemistry at a glance. John Wiley & Sons, 2012. (c) Im, Y.; Byun, S. Y.; Kim, J. H.; Lee, D. R.; Oh, C. S.; Yook, K. S.; Lee, J. Y. Recent Progress in High-Efficiency Blue-Light-Emitting Materials for Organic Light-Emitting Diodes. *Adv. Funct. Mater.* **2017,** *27*, 1603007.
2. (a) Wu, X.-F., ed. Transition Metal-catalyzed Heterocycle Synthesis via C-H Activation. John Wiley & Sons, 2015. (b) Scriven, E. F. V.; Ramsden, C. A. eds. Advances in Heterocyclic Chemistry. Elsevier, 2017, *123*, 1.
3. (a) Majumdar, K. C.; and Chattopadhyay, S. K. eds. *Heterocycles in natural product synthesis*. John Wiley & Sons, 2011. (b) Eicher, T.; Hauptmann, S.; Speicher, A. The Chemistry of Heterocycles: Structures, Reactions, Synthesis, and Applications. John Wiley & Sons, 2013.
4. For reviews on ring expansion reactions, see: (a) D´hooghe, M.; Ha, H.-J. Synthesis of 4-to 7-membered Heterocycles by Ring Expansion. *Top. Heterocycl. Chem.* **2016,** *41*, 311. (b) Bull, J. A.; Croft, R. A.; Davis, O. A.; Doran, R.; Morgan, K. F. Oxetanes: Recent Advances in Synthesis, Reactivity, and Medicinal Chemistry. *Chem. Rev.* **2016,** *116*, 12150. (c) Donald, J. R.; Unsworth, W. P. Ring-Expansion Reactions in the Synthesis of Macrocycles and Medium-Sized Rings. *Chem. Eur. J.* **2017,** *23*, 8780.
5. For books and reviews on cycloreversion of 5, 6-membered heterocycles, see: (a) Van der Plas, H. C. Advances in Heterocyclic Chemistry. Elsevier, 1999, *74*, 1. (b) Katritzky, A. R.; Ramsden, C. A.; Scriven, E. F. V.; Taylor, R. J. K., Eds. Comprehensive Heterocyclic Chemistry III; Pergamon: Oxford, UK, 2008. (c) Hajós, G.; Riedl, Z.; Kollenz, G. Recent Advances in Ring Transformations of Five-Membered Heterocycles and Their Fused Derivatives. *Eur. J. Org. Chem.* **2001,** 3405.
6. (a) Landais, Y. eds. Free-Radical Synthesis and Functionalization of Heterocycles. Top. Heterocycl. Chem. Springer, 2018, 54. (b) Das, R.; Kapur, M. Transition-Metal-Catalyzed C−H Functionalization Reactions of π-Deficient Heterocycles. *Asian J. Org. Chem.* **2018,** 7, 1217.
7. For relevant reviews on photocatalysis, see: (a) Stephenson, C. R. J.; Yoon, T. R.; MacMillan, D. W. C. eds. Visible Light Photocatalysis in Organic Chemistry. John Wiley & Sons, 2018. (b) D. Cambié, C. Bottecchia, N. J. W. Straathof, V. Hessel, T. Noël, Applications of Continuous-Flow Photochemistry in Organic Synthesis, Material Science, and Water Treatment. *Chem. Rev.* **2016,** *116*, 10276. (c) Romero, N. A.; Nicewicz, D. A. Organic Photoredox Catalysis. *Chem. Rev.* **2016,** *116*, 10075. (d) Marzo, L.; Pagire, S. K.; Reiser, O.; König, B. Visible-Light Photocatalysis: Does It Make a Difference in Organic Synthesis? *Angew. Chem. Int. Ed.* **2018**, *57*, 10034.
8. For our previous contributions in the area, see: (a) Iqbal, N.; Jung, J.; Park, S.; Cho, E. J. Controlled Trifluoromethylation Reactions of Alkynes through Visible-Light Photoredox Catalysis. *Angew. Chem. Int. Ed.* **2014,** *53*, 539. (b) Choi, S.; Chatterjee, T.; Choi, W. J.; You, Y.; Cho, E. J. Synthesis of Carbazoles by a Merged Visible Light Photoredox and Palladium-Catalyzed Process. *ACS Catal.* **2015,** *5*, 4796. (c) Chatterjee, T.; Iqbal, N.; You, Y.; Cho, E. J. Controlled Fluoroalkylation Reactions by Visible-Light Photoredox Catalysis. *Acc. Chem. Res.* **2016,** *49*, 2284.
9. For reviews and perspective on photocatalytic N-radical generation, see: (a) Chen, J.-R.; Hu, X.-Q.; Lu, L.-Q.; Xiao, W.-J. Visible light photoredox-controlled reactions of N-radicals and radical ions. *Chem. Soc. Rev.* **2016,** *45*, 2044. (b) Xiong, T.; Zhang, Q. New amination strategies based on nitrogen-centered radical chemistry. *Chem. Soc. Rev.* **2016,** *45*, 3069. (c) Kärkäs, M. D. Photochemical Generation of Nitrogen-Centered Amidyl, Hydrazonyl, and Imidyl Radicals: Methodology Developments and Catalytic Applications. *ACS Catal.* **2017,** *7*, 4999.
10. For selected examples on utilizing N-H bond in N-radical generation, see: (a) Hu, X.-Q.; Chen, J.-R.; Wei, Q.; Liu, F.-L.; Deng, Q.-H.; Beauchemin, A. M.; Xiao, W.-J. Photocatalytic generation of N-centered hydrazonyl radicals: a strategy for hydroamination of β,γ-unsaturated hydrazones. *Angew. Chem., Int. Ed.* **2014,** *53*, 12163. (b) Choi, G. J.; Knowles, R. R. Catalytic Alkene Carboaminations Enabled by Oxidative Proton-Coupled Electron Transfer. *J. Am. Chem. Soc.* **2015,** *137*, 9226. (c) Choi, G. J.; Zhu, Q.; Miller, D. C.; Gu, C. J.; Knowles, R. R. Catalytic alkylation of remote C–H bonds enabled by proton-coupled electron transfer. *Nature* **2016,** *539*, 268. (d) Chu, J. C. K.; Rovis, T. Amide-directed photoredox-catalysed C–C bond formation at unactivated sp3 C–H bonds. *Nature* **2016,** *539*, 272. (e) Wappes, E. A.; Nakafuku, K. M.; Nagib, D. A. Directed β C–H Amination of Alcohols via Radical Relay Chaperones. *J. Am. Chem. Soc.* **2017,** *139*, 10204. (f) Shu, W.; Genoux, A.; Li, Z.; Nevado, C. γ -Functionalizations of Amines through Visible-Light-Mediated, Redox-Neutral C–C Bond Cleavage. *Angew. Chem. Int. Ed.* **2017,** *56*, 10521. (g) Becker, P.; Duhamel, T.; Stein, C. J.; Reiher, M.; Muñiz, K. Cooperative Light-Activated Iodine and Photoredox Catalysis for the Amination of Csp^3–H Bonds. *Angew. Chem. Int. Ed.* **2017**, *56*, 8004. (h) Zhu, Q.; Graff, D. E.; Knowles, R. R. Intermolecular Anti-Markovnikov Hydroamination of Unactivated Alkenes with Sulfonamides Enabled by Proton-Coupled Electron Transfer. *J. Am. Chem. Soc.* **2018,** *140*, 741. (i) Morcillo, S. P.; Dauncey, E. M.; Kim, J. H.; Douglas, J. J.; Sheikh, N. S.; Leonori, D. Photoinduced Remote Functionalization of Amides and Amines Using Electrophilic Nitrogen Radicals. *Angew. Chem. Int. Ed.* **2018**, *57*, 12945. (j) Jia, J.; Ho, Y. A.; Below, R. F.; Rueping, M. Brønsted Base Assisted Photoredox Catalysis: Proton Coupled Electron Transfer for Remote C–C Bond Formation via Amidyl Radicals. *Chem. Eur. J.* **2018**, *24*, 14054. (k) Moon, Y.; Jang, E.; Choi, S.; Hong, S. Visible-Light-Photocatalyzed Synthesis of Phenanthridinones and Quinolinones via Direct Oxidative C–H Amidation. *Org. Lett.* **2018**, *20*, 240. (l) Wu, K.; Wang, L.; Colón-Rodríguez, S.; Flechsig, G.-U.; Wang, T. Amidyl Radical Directed Remote Allylation of Unactivated sp3 C-H Bonds by Organic Photoredox Catalysis. *Angew. Chem. Int. Ed.* **2019**, *58*, 1774.
11. For selected examples on photocatalytic *N*-radical cascade reactions, see: (a) Hu, X.-Q.; Qi, X.-T.; Chen, J.-R.; Zhao, Q.-Q.; Wei, Q.; Lan, Y.; Xiao, W.-J. Catalytic N-radical cascade reaction of hydrazones by oxidative deprotonation electron transfer and TEMPO mediation. *Nat. Commun.* **2016,** *7*, 11188. (b) Morris, S. A.; Wang, J.; Zheng, N. The Prowess of Photogenerated Amine Radical Cations in Cascade Reactions: From Carbocycles to Heterocycles. *Acc. Chem. Res.* **2016,** *49*, 1957. (c) Zheng, S.; Gutiérrez-Bonet, Á.; Molander, G. A. Merging Photoredox PCET with Ni-Catalyzed Cross-Coupling: Cascade Amidoarylation of Unactivated Olefins. *Chem* **2019**, *5*, 339.
12. For selected examples on photocatalytic *N*-radical generation by N-N, N-O and N-X bond cleavages, see: (a)

Kim, H.; Kim, T.; Lee, D. G.; Roh, S. W.; Lee, C. Nitrogen-centered radical-mediated C–H imidation of arenes and heteroarenes via visible light induced photocatalysis. *Chem. Commun.* **2014**, *50*, 9273. (c) Walton, J. C. Synthetic Strategies for 5- and 6-Membered Ring Azaheterocycles Facilitated by Iminyl Radicals. Molecules **2016,** *21,* 660. (e) Jiang, H.; Studer, A. Iminyl-Radicals by Oxidation of α-Imino-oxy Acids: Photoredox-Neutral Alkene Carboimination for the Synthesis of Pyrrolines. *Angew. Chem. Int. Ed.* **2017,** *56*, 12273. (g) Wang, H.; Zhang, D.; Bolm, C. Sulfoximidations of Benzylic C-H bonds by Photocatalysis. *Angew. Chem. Int. Ed.* **2018**, *57*, 5863. (h) Zhang, D.; Wang, H.; Bolm, C. Photocatalytic difunctionalisations of alkenes with N-SCN sulfoximines. *Chem. Commun.* **2018**, *54*, 5772. (i) Dauncey, E. M.; Morcillo, S. P.; Douglas, J. J.; Sheikh, N. S.; Leonori, D. Photoinduced Remote Functionalisations by Iminyl Radical Promoted C-C and C-H Bond Cleavage Cascades. *Angew. Chem. Int. Ed.* **2018**, *57*, 744. (j) Yu, X.-Y.; Chen, J.-R.; Wang, P.-Z.; Yang, M.-N.; Liang, D.; Xiao, W.-J. A Visible-Light-Driven Iminyl Radical-Mediated C−C Single Bond Cleavage/Radical Addition Cascade of Oxime Esters. *Angew. Chem. Int. Ed.* **2018**, *57*, 738.

13. For selected examples on photocatalytic *N*-radical cascade reactions by N-N, N-O and N-X bond cleavages, see: (a) Allen, L. J.; Cabrera, P. J.; Lee, M.; Sanford, M. S. N-Acyloxyphthalimides as Nitrogen Radical Precursors in the Visible Light Photocatalyzed Room Temperature C–H Amination of Arenes and Heteroarenes. *J. Am. Chem. Soc.* **2014,** *136*, 5607. (c) Cai, S.-H.; Xie, J.-H.; Song, S.; Ye, L.; Feng, C.; Loh, T.-P. Visible-Light-Promoted Carboimination of Unactivated Alkenes for the Synthesis of Densely Functionalized Pyrroline Derivatives. *ACS Catal.* **2016,** *6*, 5571. (g) Jiang, H.; Studer, A. Amidyl Radicals by Oxidation of α-Amido-oxy Acids: Transition-Metal-Free Amidofluorination of Unactivated Alkenes. *Angew. Chem. Int. Ed.* **2018,** *57*, 10707. (h) Dauncey, E. M.; Morcillo, S. P.; Douglas, J. J.; Sheikh, N. S.; Leonori, D. Photoinduced Remote Functionalisations by Iminyl Radical Promoted C-C and C-H Bond Cleavage Cascades. *Angew. Chem. Int. Ed.* **2018**, *130*, 752. (i) Nakafuku, K. M.; Fosu, S. C.; Nagib, D. A. Catalytic Alkene Difunctionalization via Imidate Radicals. *J. Am. Chem. Soc.* **2018**, *140*, 11202.
14. (a) Buscemi, S.; Vivona, N.; Caronna, T. Photoinduced Molecular Rearrangements. The Photochemistry of Some 1,2,4-Oxadiazoles in the Presence of Nitrogen Nucleophiles. Formation of 1,2,4-Triazoles, Indazoles, and Benzimidazoles. *J. Org. Chem.* **1996**, *61*, 8397. (b) Buscemi, S.; Pace, A.; Vivona, N.; Caronna, T.; Galia, A. Photoinduced Single Electron Transfer on 5-Aryl-1,2,4-oxadiazoles: Some Mechanistic Investigations in the Synthesis of Quinazolin-4-ones. *J. Org. Chem.* **1999**, *64*, 7028. (c) Pace, A.; Buscemi, S.; Vivona, N. Heterocyclic Rearrangements in Constrained Media. A Zeolite-Directed Photorearrangement of 1,2,4-Oxadiazoles. *J. Org. Chem.* **2005**, *70*, 2322. (d) Pace, A.; Pierro, P. The new era of 1,2,4-oxadiazoles. *Org. Biomol. Chem.* **2009**, *7*, 4337.
15. For other non-photocatalytic examples, see: (a) Natale, N. R. Selective reduction of isoxazoles with samarium diiodide. *Tetrahedron Lett.* **1982,** *23*, 5009. (b) Janza, B.; Studer, A. Stereoselective Cyclization Reactions of IBX-Generated Alkoxyamidyl Radicals. *J. Org. Chem.*, **2005**, *70*, 6991. (c) Wang, Y.-F.; Zhang, F.-L.; Chiba, S. Oxidative Radical Skeletal Rearrangement Induced by Molecular Oxygen: Synthesis of Quinazolinones. *Org. Lett.* **2013,** *15*, 2842.
16. (a) Larraufie, M.-H.; Courillon, C.; Ollivier, C.; Lacôte, E.; Malacria, M.; Fensterbank, L. Radical Migration of Substituents of Aryl Groups on Quinazolinones Derived from N-Acyl Cyanamides. *J. Am. Chem. Soc.* **2010**, *132*, 4381. (b) Larraufie, M.-H.; Ollivier, C.; Fensterbank, L.; Malacria, M. Radical Synthesis of Guanidines from N-Acyl Cyanamides. *Angew. Chem., Int. Ed.* **2010**, *49*, 2178. (c) Beaume, A.; Courillon, C.; Derat, E.; Malacria, M. Unprecedented Aromatic Homolytic Substitutions and Cyclization of Amide-Iminyl Radicals: Experimental and Theoretical Study. *Chem. Eur. J.* **2008**, *14*, 1238. (d) Servais, A.; Azzouz, M.; Lopes, D.; Courillon, C.; Malacria, M. Radical Cyclization of N-Acylcyanamides: Total Synthesis of Luotonin A. *Angew. Chem., Int. Ed.* **2007**, *46*, 576.
17. For general reviews on oxygenation using molecular oxygen, see: (a) Bian, C.; Singh, A. K.; Niu, L.; Yi, H.; Lei, A. Visible-Light-Mediated Oxygenation Reactions using Molecular Oxygen. *Asian J. Org. Chem.* **2017,** *6*, 386. (b) Liang, Y.-F.; Jiao, N. Oxygenation via C–H/C–C Bond Activation with Molecular Oxygen. *Acc. Chem. Res.* **2017,** *50*, 1640. (c) Pibiri, I.; Buscemi, S.; Piccionello, A. P.; Pace, A. Photochemically Produced Singlet Oxygen: Applications and Perspectives. *ChemPhotoChem* **2018,** *2*, 535.
18. For selected examples, see: (a) Chiba, S.; Zhang, L.; Lee, J.-Y. Copper-Catalyzed Synthesis of Azaspirocyclohexadienones from α-Azido-N-arylamides under an Oxygen Atmosphere. *J. Am. Chem. Soc.* **2010,** *132*, 7266. (b) Tnay, Y. L.; Chen, C.; Chua, Y. Y.; Zhang, L.; Chiba, S. Copper-Catalyzed Aerobic Spirocyclization of Biaryl-N-H-imines via 1,4-Aminooxygenation of Benzene Rings. *Org. Lett.* **2012,** *14*, 3550. (c) Farndon, J. J.; Ma, X.; Bower, J. F. Transition Metal Free C–N Bond Forming Dearomatizations and Aryl C–H Aminations by in Situ Release of a Hydroxylamine-Based Aminating Agent. *J. Am. Chem. Soc.* **2017,** *139*, 14005. (d) Ma, X.; Farndon, J. J.; Young, T. A.; Fey, N.; Bower, J. F. A Simple and Broadly Applicable C–N Bond Forming Dearomatization Protocol Enabled by Bifunctional Amino Reagents. *Angew. Chem. Int. Ed.* **2017,** *56*, 14531.
19. For some recent reviews on dearomatization of arenes, see: (a) Roche, S. P.; Porco Jr., J. A. Dearomatization Strategies in the Synthesis of Complex Natural Products. *Angew. Chem. Int. Ed.* **2011,** *50*, 4068. (b) Wu, W.-T.; Zhang, L.; You, S.-L. Catalytic asymmetric dearomatization (CADA) reactions of phenol and aniline derivatives. *Chem. Soc. Rev.* **2016,** *45*, 1570. (c) Reddy, C. R.; Prajapti, S. K.; Warudikar, K.; Ranjan, R.; Rao, B. B. *ipso*-Cyclization: an emerging tool for multifunctional spirocyclohexadienones. *Org. Biomol. Chem.* **2017,** *15*, 3130.
20. For diazaspiro compounds as GlyT1 transporter inhibitors, see: (a) Dean, A. W.; Porter, R. A. Glyt1 transporter inhibitors and uses thereof in treatment of neurological and neuropsychiatric disorders. WO Patent 2007014762, 2007. (b) Marshall, H. R. Glyt1 transporter inhibitors and uses thereof in treatment of neurological and neuropsychiatric disorders. WO Patent 2008092879, 2008.
21. The transition-metal-catalyzed dearomative spirocyclization strategies usually involve functionalized alkoxyarenes, including phenol derivatives.
22. The oxidation of oxadiazolines at high temperature by triplet oxygen was proposed via N-radical formation; see (ref 15c).
23. Even the reaction of **1a** with a highly oxidizing TPPT catalyst was inefficient.
24. The triplet energies were calculated considering the solvation effect of DMSO using M06-2X / 6-311++G** method (see Figure S5 for details).
25. Blum, T. R.; Miller, Z. D.; Bates, D. M.; Guzei, I. A.; Yoon, T. P. Enantioselective photochemistry through Lewis acid–catalyzed triplet energy transfer. *Science*, **2016,** *354*, 1391.

26. Turro, N. J. Modern Molecular Photochemistry, University Science Books, Sausalito, California, 1991.
27. Sagadevan, A.; Hwang, K. C.; Su, M.-D. Singlet oxygen-mediated selective C–H bond hydroperoxidation of ethereal hydrocarbons. *Nature Commun.* **2017**, 8, 1812.
28. The reaction of **1a** was performed under standard conditions for 3 h and then in the dark for additional 15 h.
29. Aubry, J. M. Search for Singlet Oxygen in the Decomposition of Hydrogen Peroxide by Mineral Compounds in Aqueous Solutions. *J. Am. Chem. Soc.* **1985**, *107*, 5844.
30. (a) Beckwith, A. L. J. The mechanisms of the rearrangements of allylic hydroperoxides: 5α-hydroperoxy-3β-hydroxycholest-6-ene and 7α-hydroperoxy-3β-hydroxycholest-5-ene. *J. Chem. Soc., Perkin Trans. 2*, **1989**, 815. (b) Porter, N. A.; Wujek, J. S. Allylic hydroperoxide rearrangement. β-Scission or concerted pathway? *J. Org. Chem.* **1987**, *52*, 5085.
31. A peroxide indicator, QUANTOFIX Peroxid 25, was used.
32. CCDC 1846200 and 1846201 contain the supplementary crystallographic data for this paper, which can be obtained free of charge from The Cambridge Crystallographic Data Centre.

For Table of Content Only

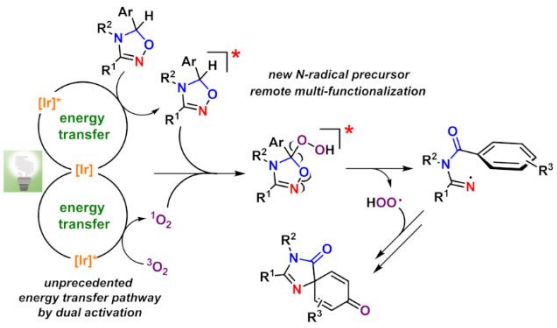

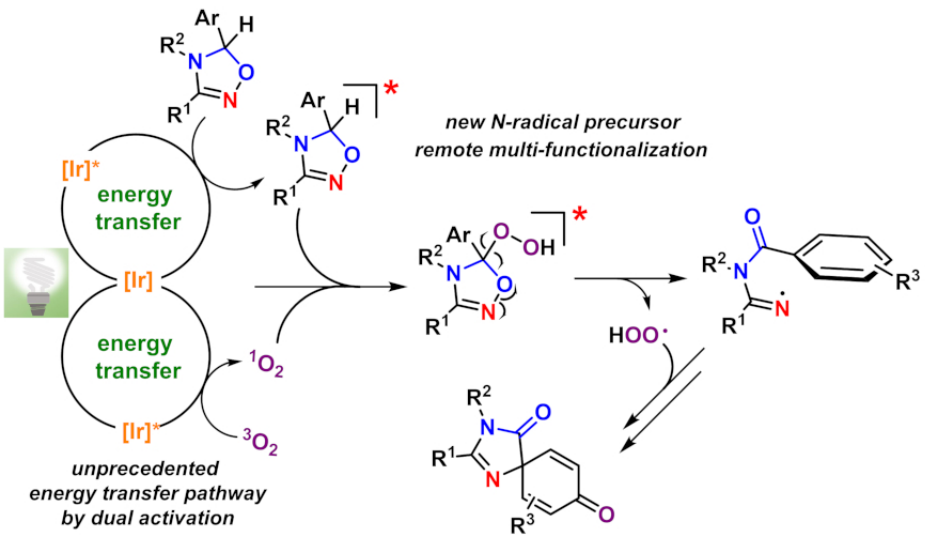

TOC

79x42mm (300 x 300 DPI)